Supporting Information

Three Cadmium Coordination Polymers with Carboxylate and Pyridine Mixed Ligands: Luminescent Sensors for Fe^{III} and Cr^{VI} Ions in an Aqueous Medium

Yanna Lin[†], *Xiaoping Zhang*[†], *Wenjie Chen*[†], *Wei Shi**[,†,‡,§] and *Peng Cheng**[,†,‡,§]

[†]College of Chemistry and Key Laboratory of Advanced Energy Materials Chemistry (MOE), Nankai University, Tianjin 300071, China

[‡]State Key Laboratory of Elemento-Organic Chemistry, Nankai University, Tianjin 300071, China

[§]Collaborative Innovation Center of Chemical Science and Engineering (Tianjin), Tianjin 300071, China

Content

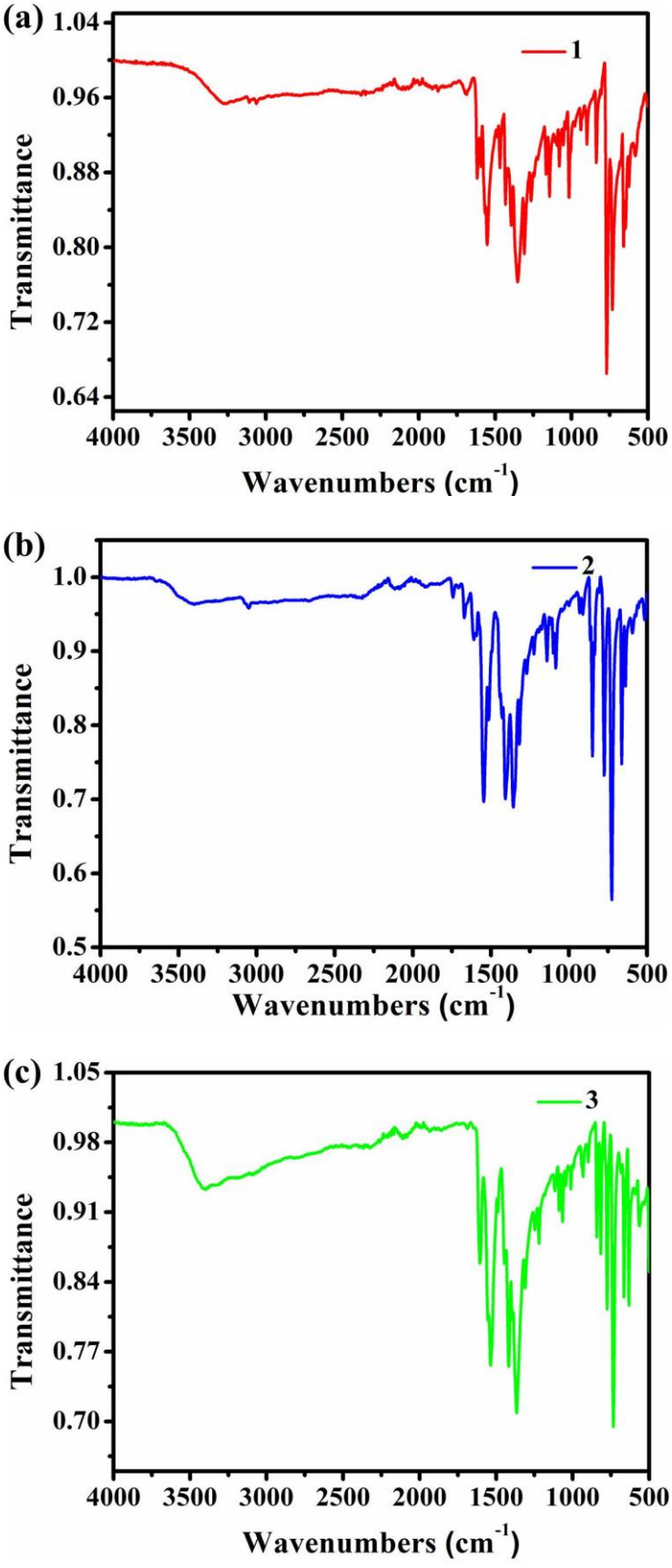

Figure S1. The FT-IR spectra of CPs **1** (a), **2** (b) and **3** (c).

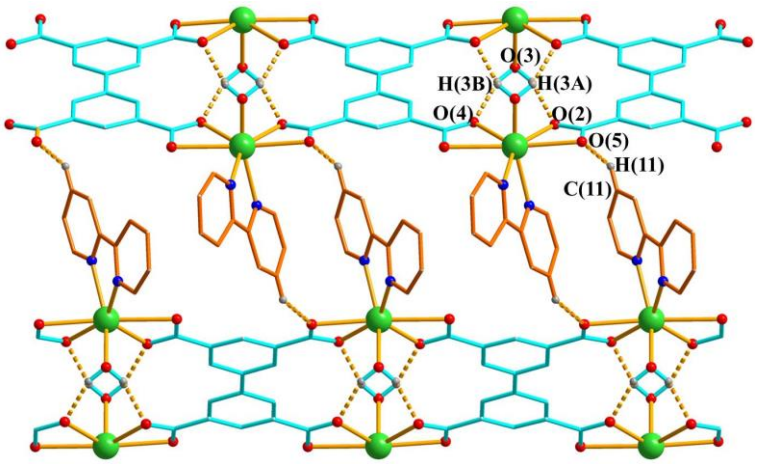

Figure S2. Two types of hydrogen bonds in **1**.

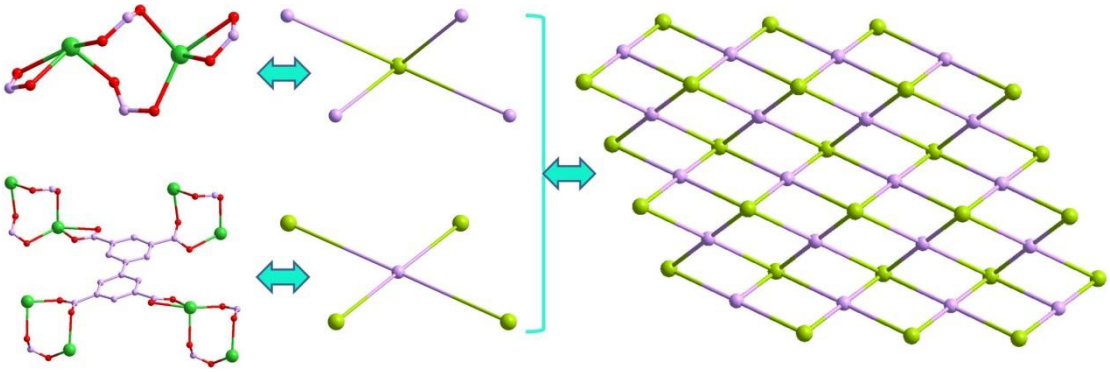

Figure S3. The simplified topological net of **2**.

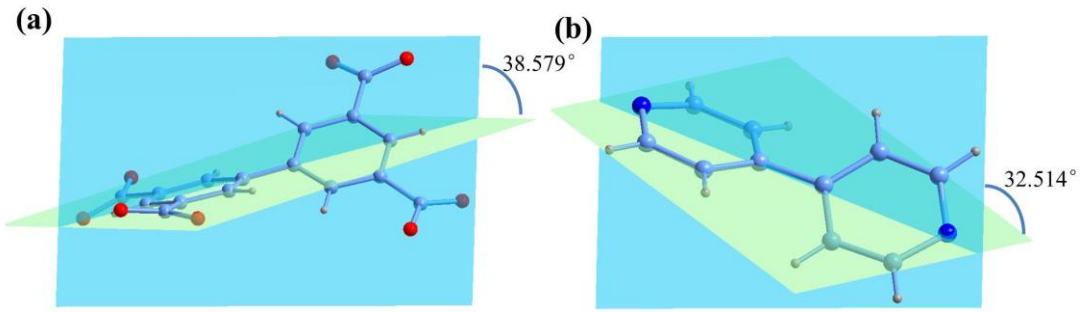

Figure S4. The dihedral angle of H_4bptc (a), 4,4'-bipy (b) in **3**.

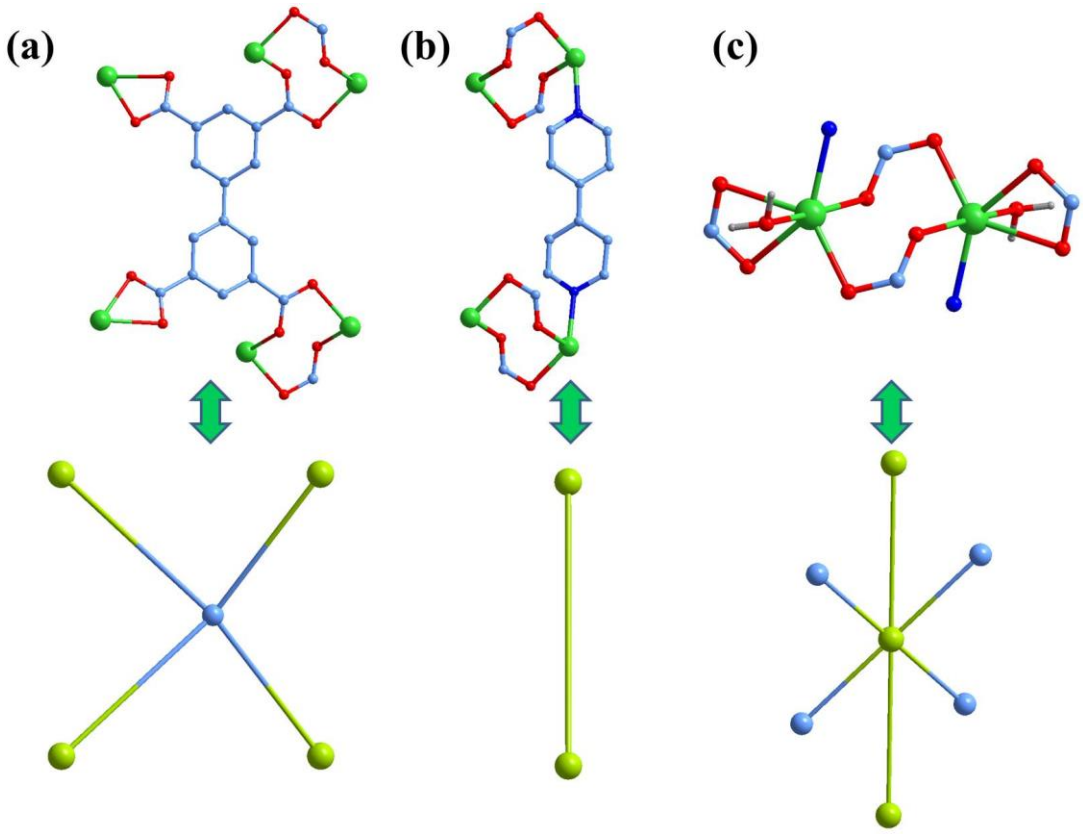

Figure S5. The representation of notes in simplified topological net of **3**.

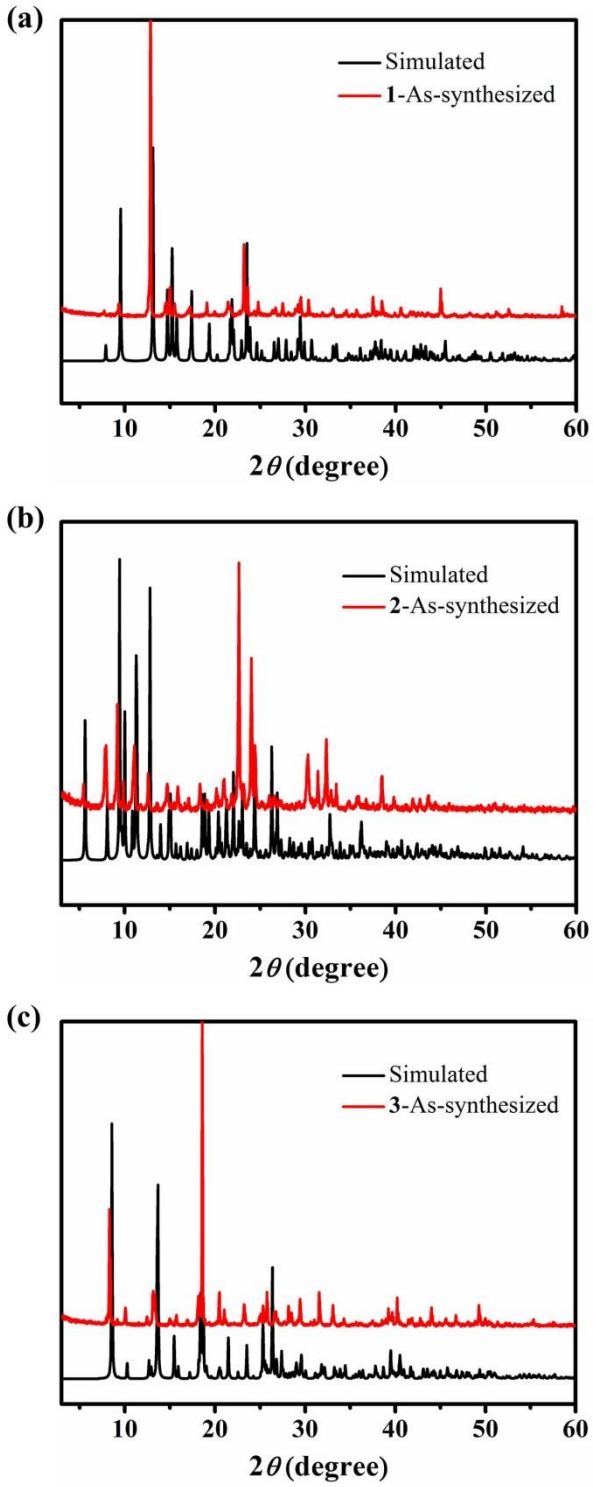

Figure S6. PXRD patterns of the synthesized samples and simulated patterns from single crystal data of CPs **1** (a), **2** (b) and **3** (c).

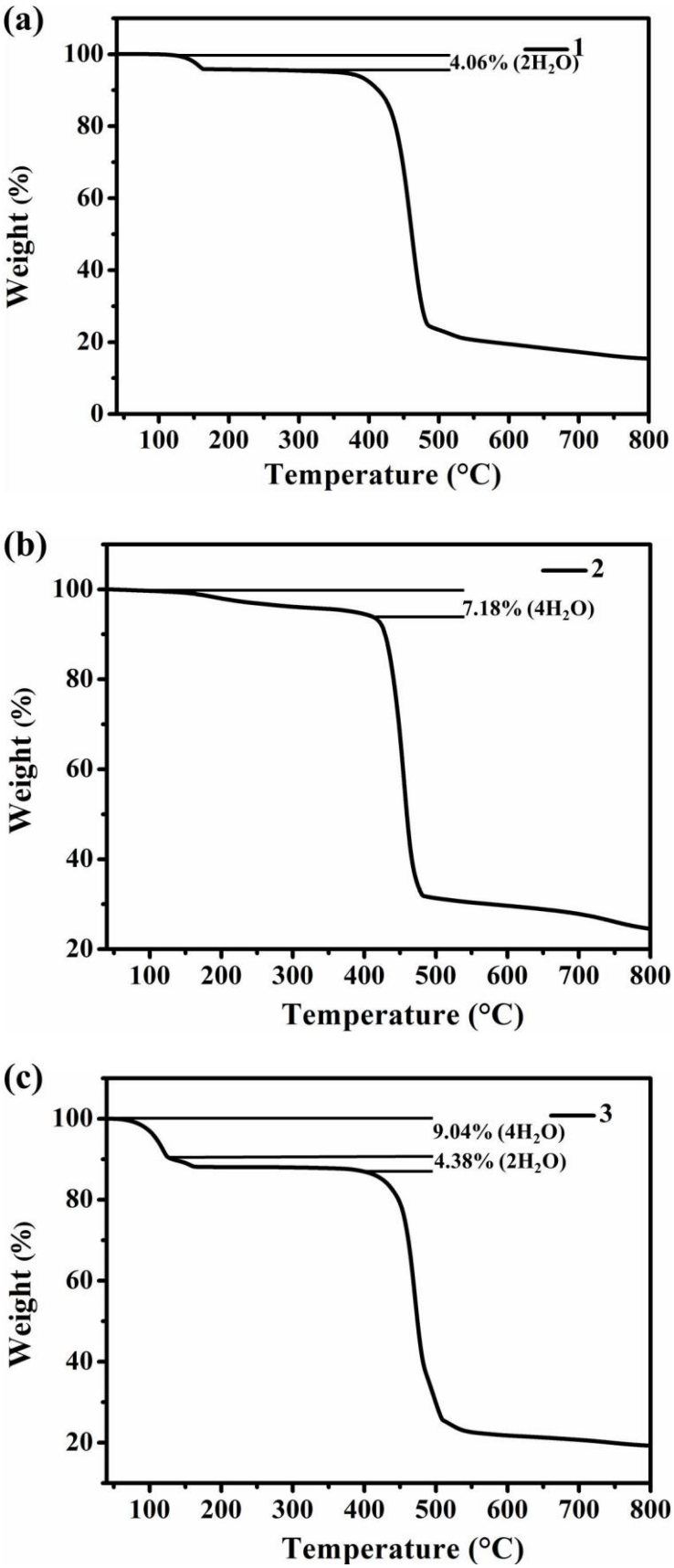

Figure S7. The TGA curves of CPs **1** (a), **2** (b) and **3** (c).

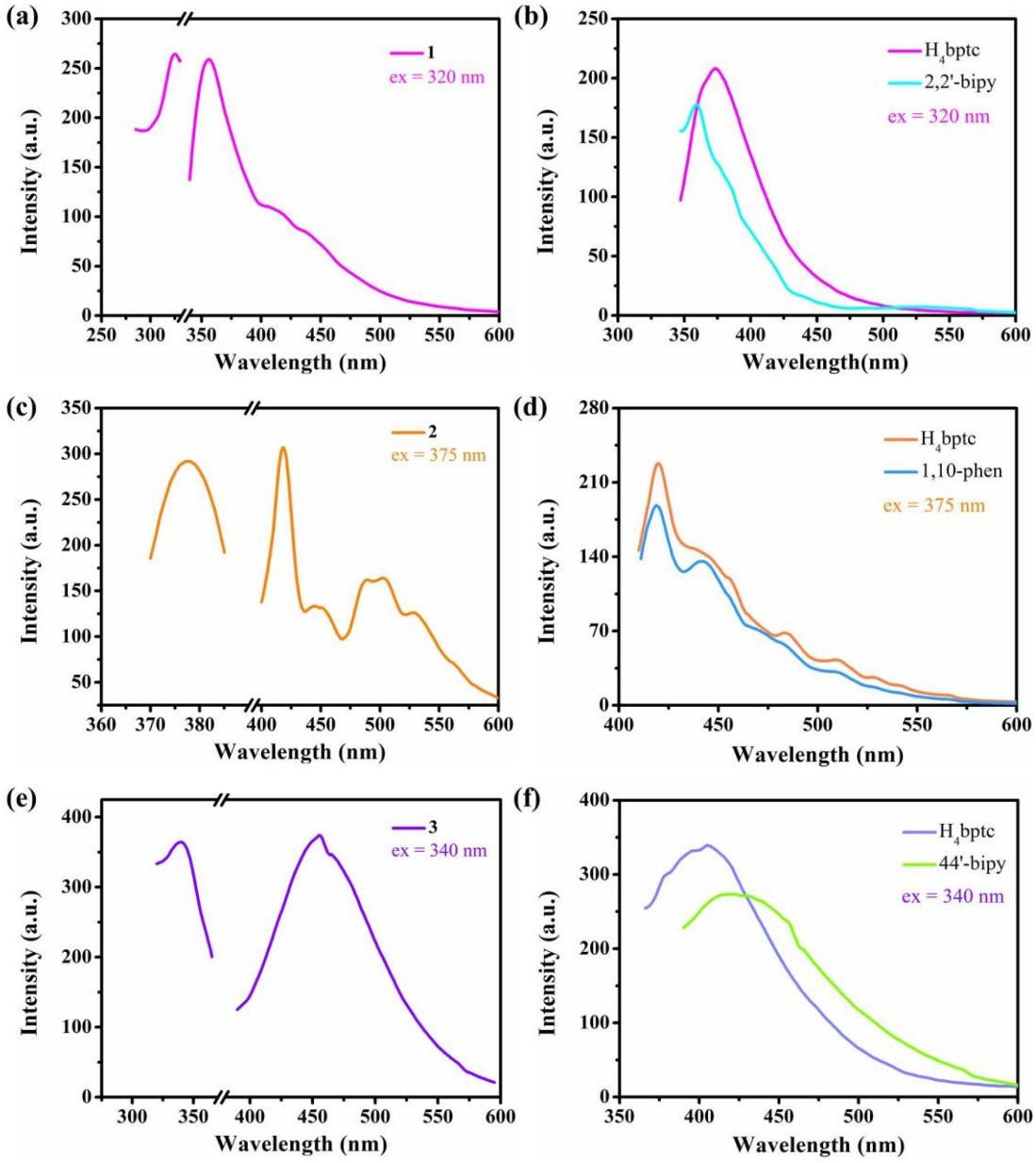

Figure S8. The room temperature solid-state excitation and emission spectra of CPs **1** (a), **2** (c), **3** (e), and the emission spectra of free ligands in CPs **1** (b), **2** (d), **3** (f), respectively.

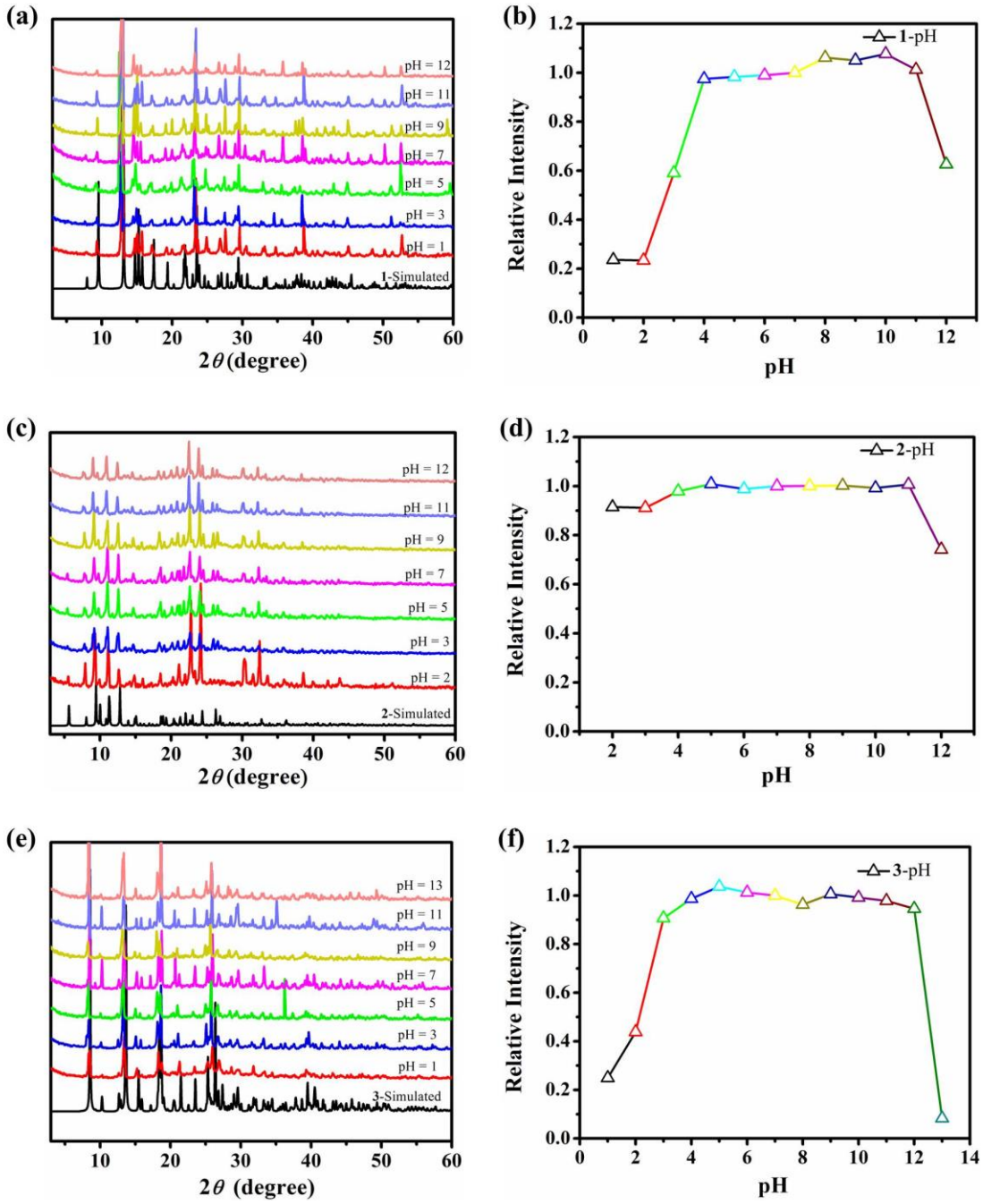

Figure S9. The PXRD patterns and the luminescent tests of CPs **1** (a) and (b), **2** (c) and (d), **3** (e) and (f) after being immersed in aqueous solution with different pH ranges, respectively.

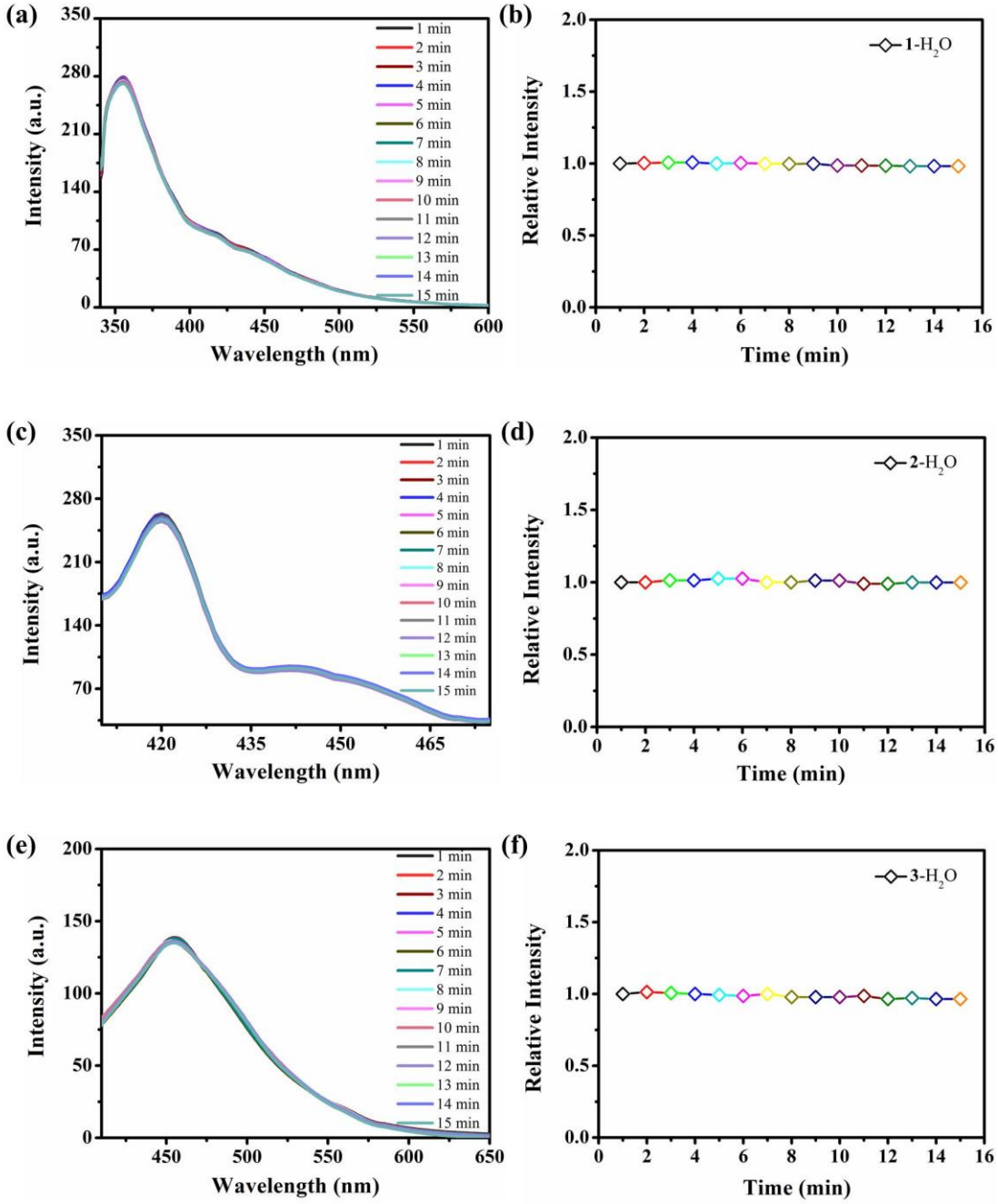

Figure S10. Time-dependent emission spectra of CPs **1** (a) and (b), **2** (c) and (d), **3** (e) and (f) suspended in aqueous solutions.

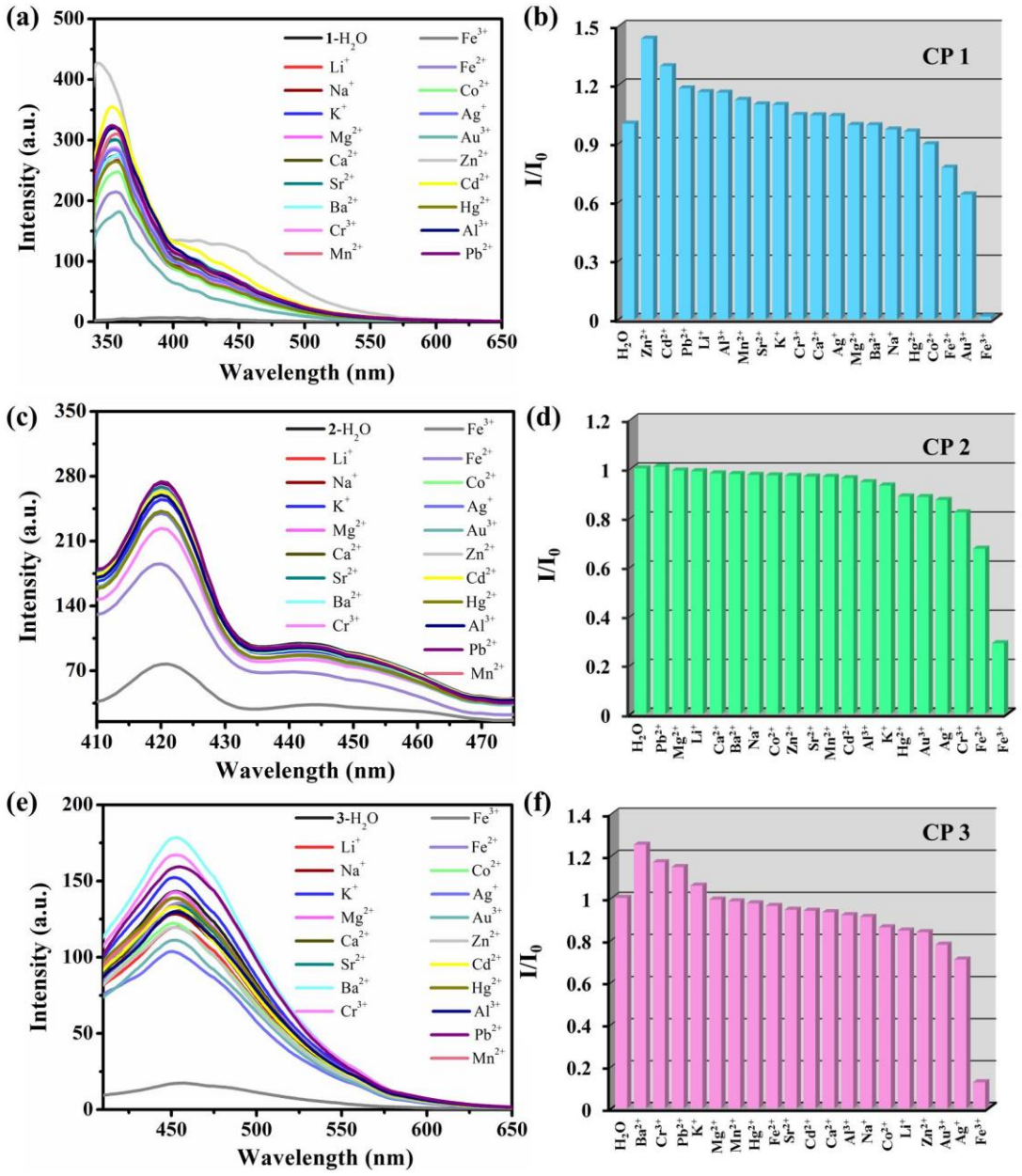

Figure S11. Suspension-state luminescent spectra of CPs **1** (a), **2** (c) and **3** (e), and the maximum emission intensities of CPs **1** (b), **2** (d) and **3** (f) with different metal cations (1×10^{-3} M).

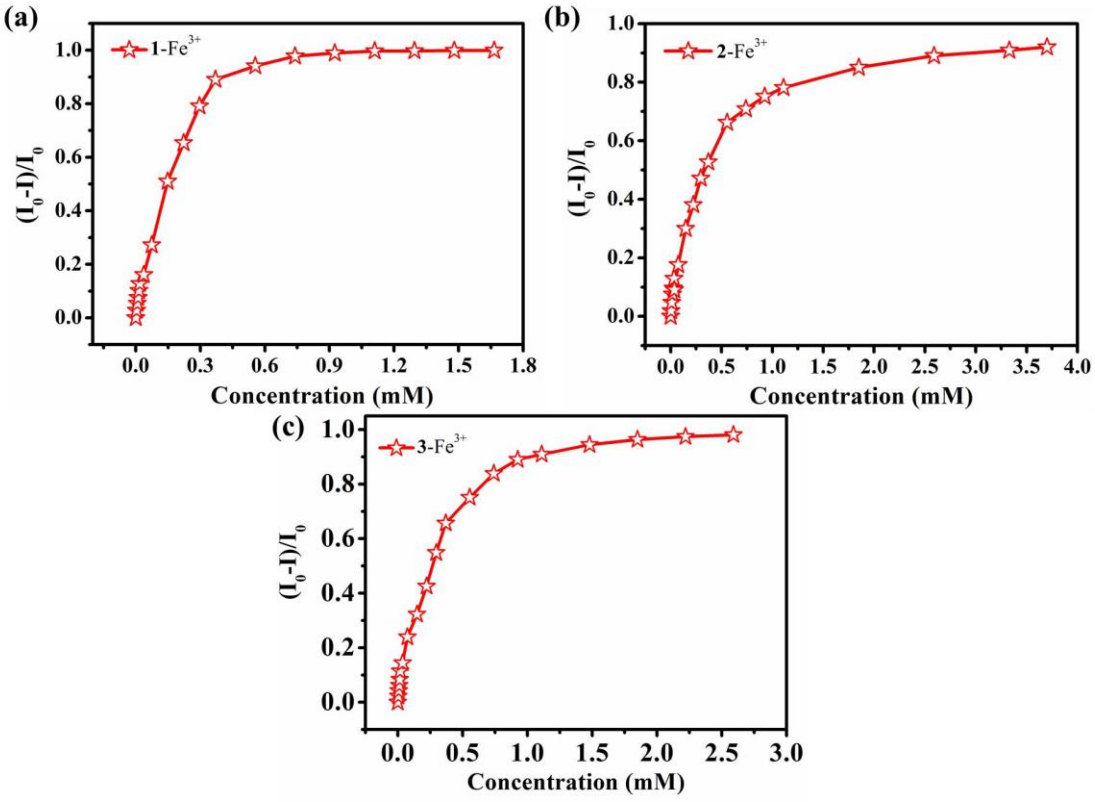

Figure S12. The quenching efficiency of CPs **1** (a), **2** (b) and **3** (c), in aqueous solution with different concentrations of Fe^{3+} ions.

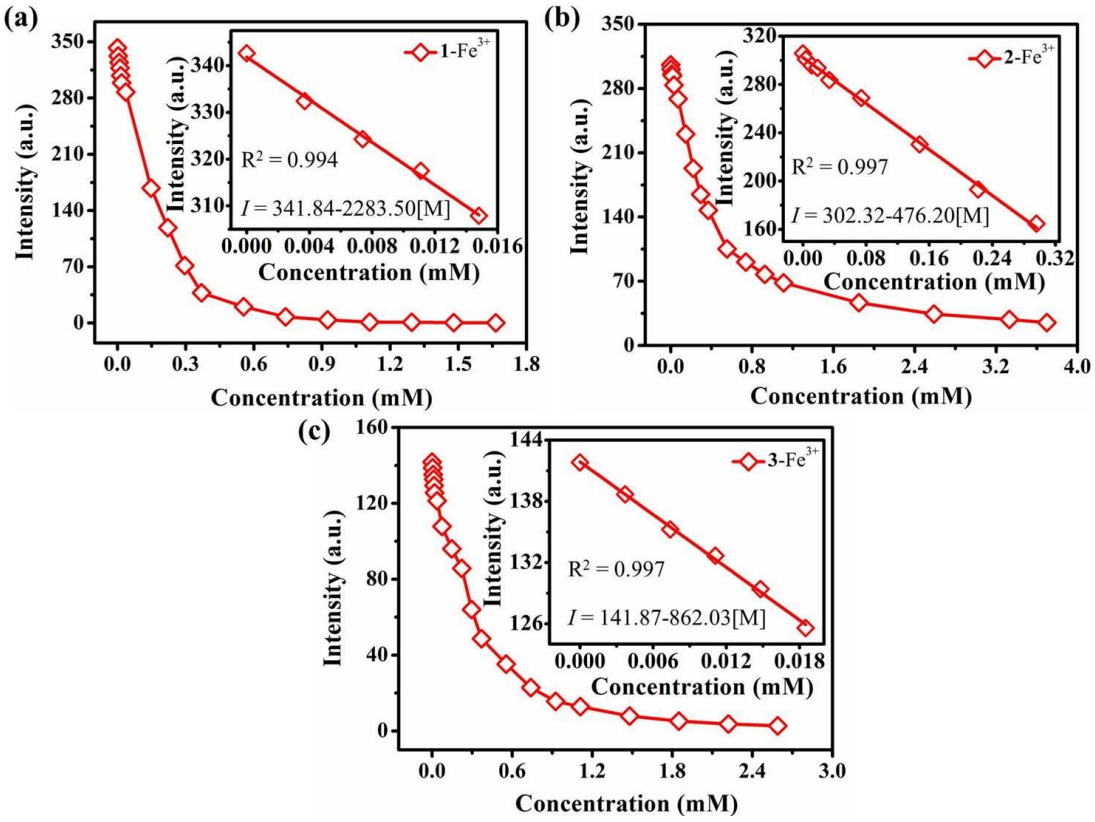

Figure S13. Changes of luminescent intensities with the maximum emission peaks of CPs **1** (a), **2** (b) and **3** (c), in aqueous solution with increasing concentrations of Fe^{3+} ions., insets display the linear relationships between intensities and the lower concentrations.

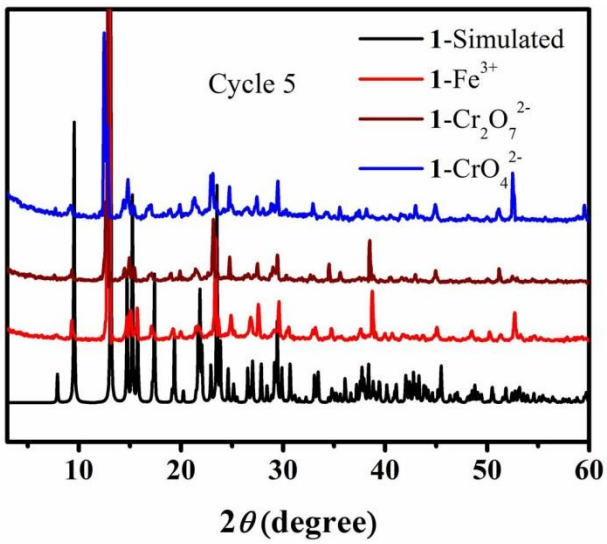

Figure S14. The PXRD patterns of CPs **1** after five cycles tests.

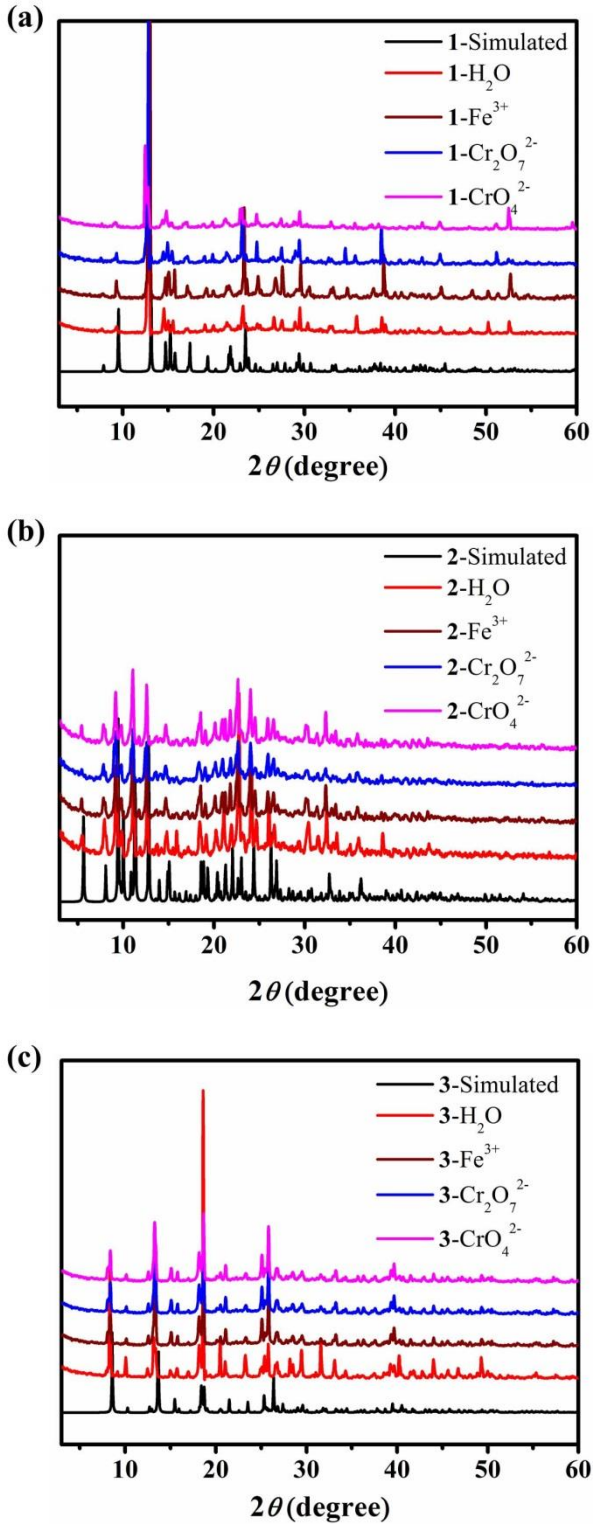

Figure S15. The PXRD patterns of CPs **1** (a), **2** (b) and **3** (c) after sensing for Fe^{3+}, $Cr_2O_7^{2-}$ and CrO_4^{2-} ions in aqueous solution.

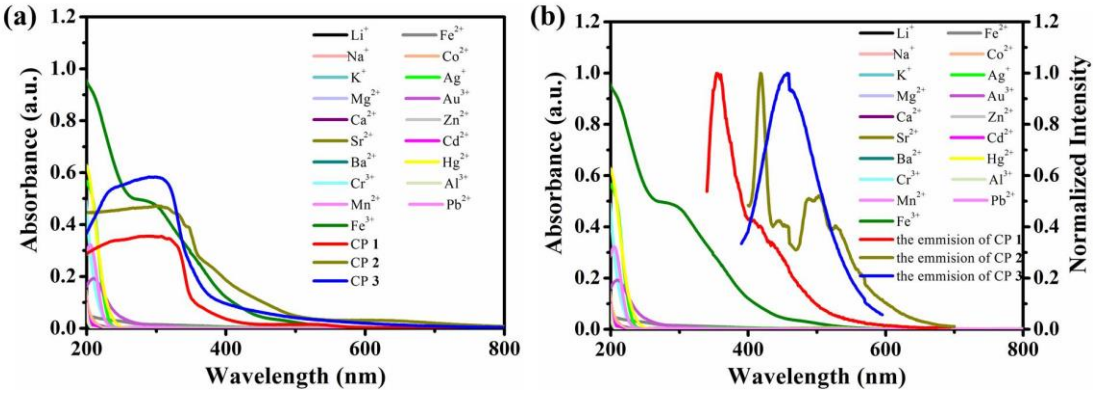

Figure S16. (a) The UV-vis absorption spectra of different metal cations in their aqueous solutions and the Solid state UV-vis absorption spectra of CPs **1**-**3**; (b) Spectral overlap between the UV-vis absorption spectra of spectra of different metal cations solutions and emission spectra of CPs **1**-**3** in water.

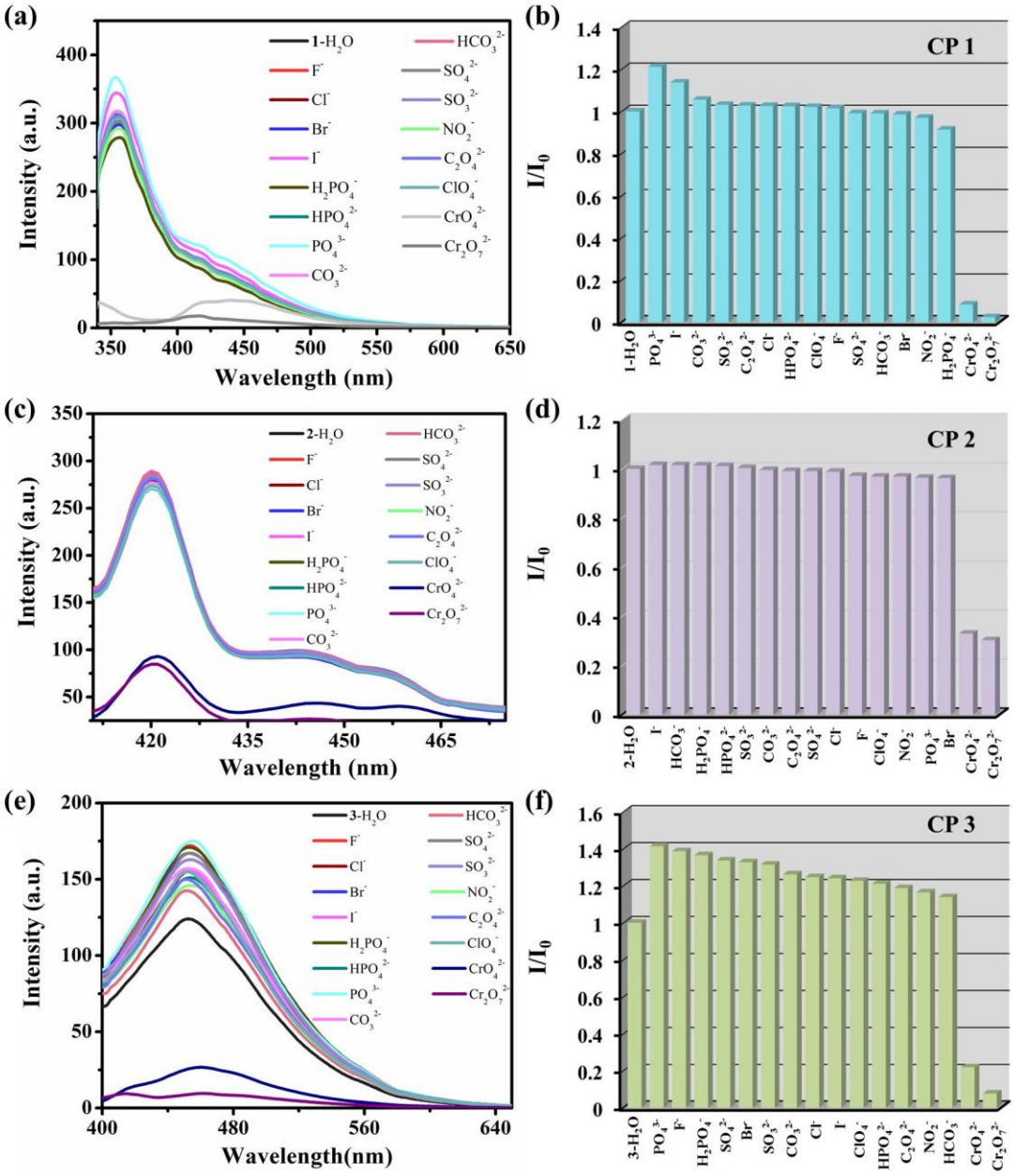

Figure S17. Suspension-state luminescent spectra of CPs **1** (a), **2** (c) and **3** (e), and the maximum emission intensities of CPs **1** (b), **2** (d) and **3** (f) with various anions (1×10^{-3} M).

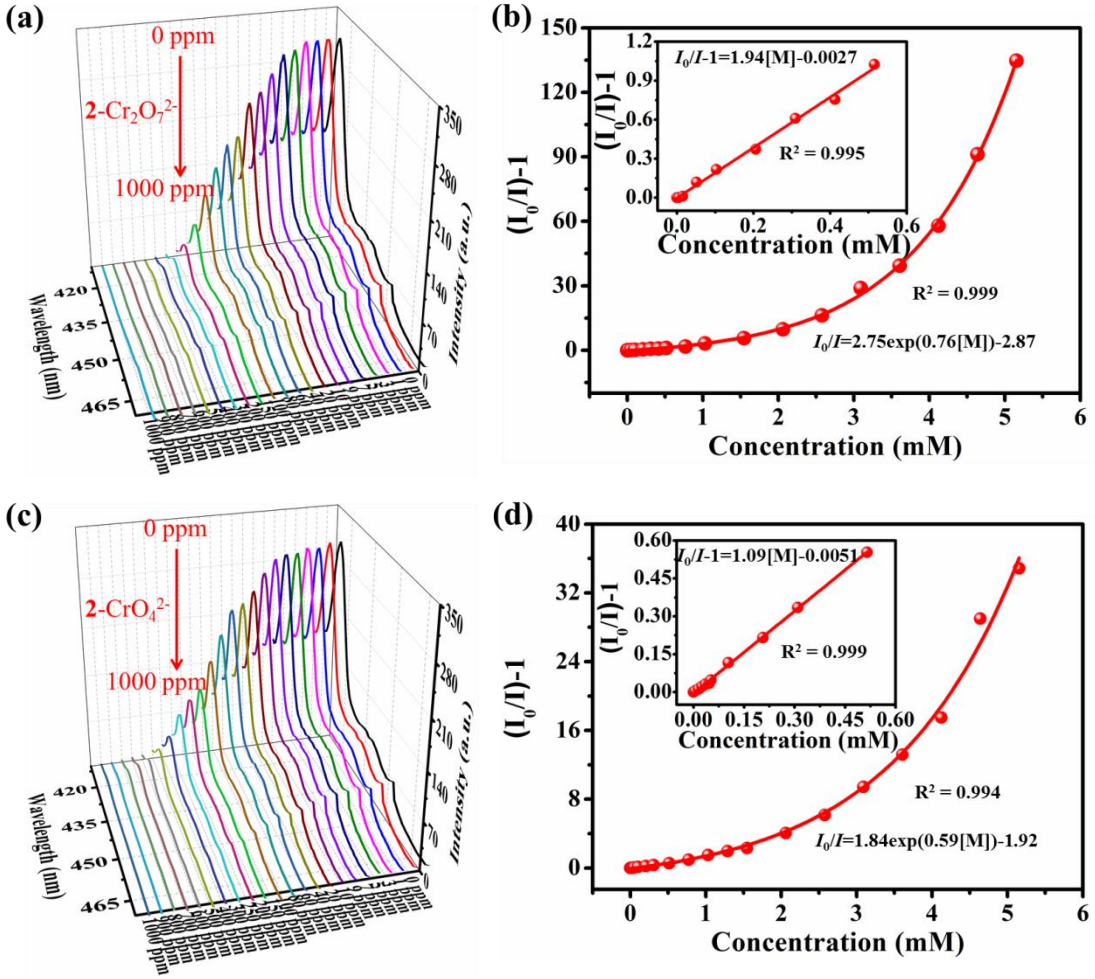

Figure S18. The emmision spectra of **2** in aqueous solution with different concentrations of $Cr_2O_7^{2-}$ (a) and CrO_4^{2-} (c) ions and the SV plots for $Cr_2O_7^{2-}$ (b) and CrO_4^{2-} (d) ions.

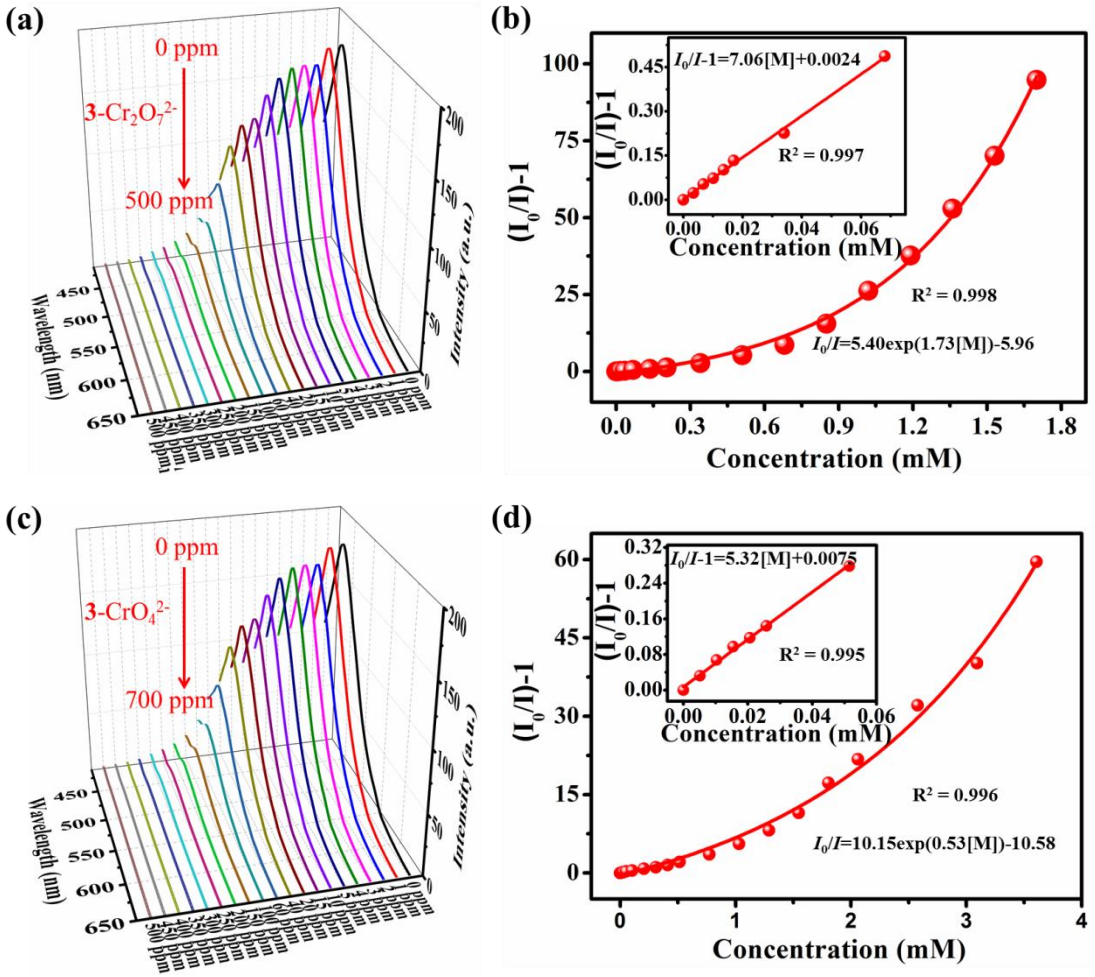

Figure S19. The emmision spectra of **3** in aqueous solution with different concentrations of $Cr_2O_7^{2-}$ (a) and CrO_4^{2-} (c) ions and the SV plots for $Cr_2O_7^{2-}$ (b) and CrO_4^{2-} (d) ions.

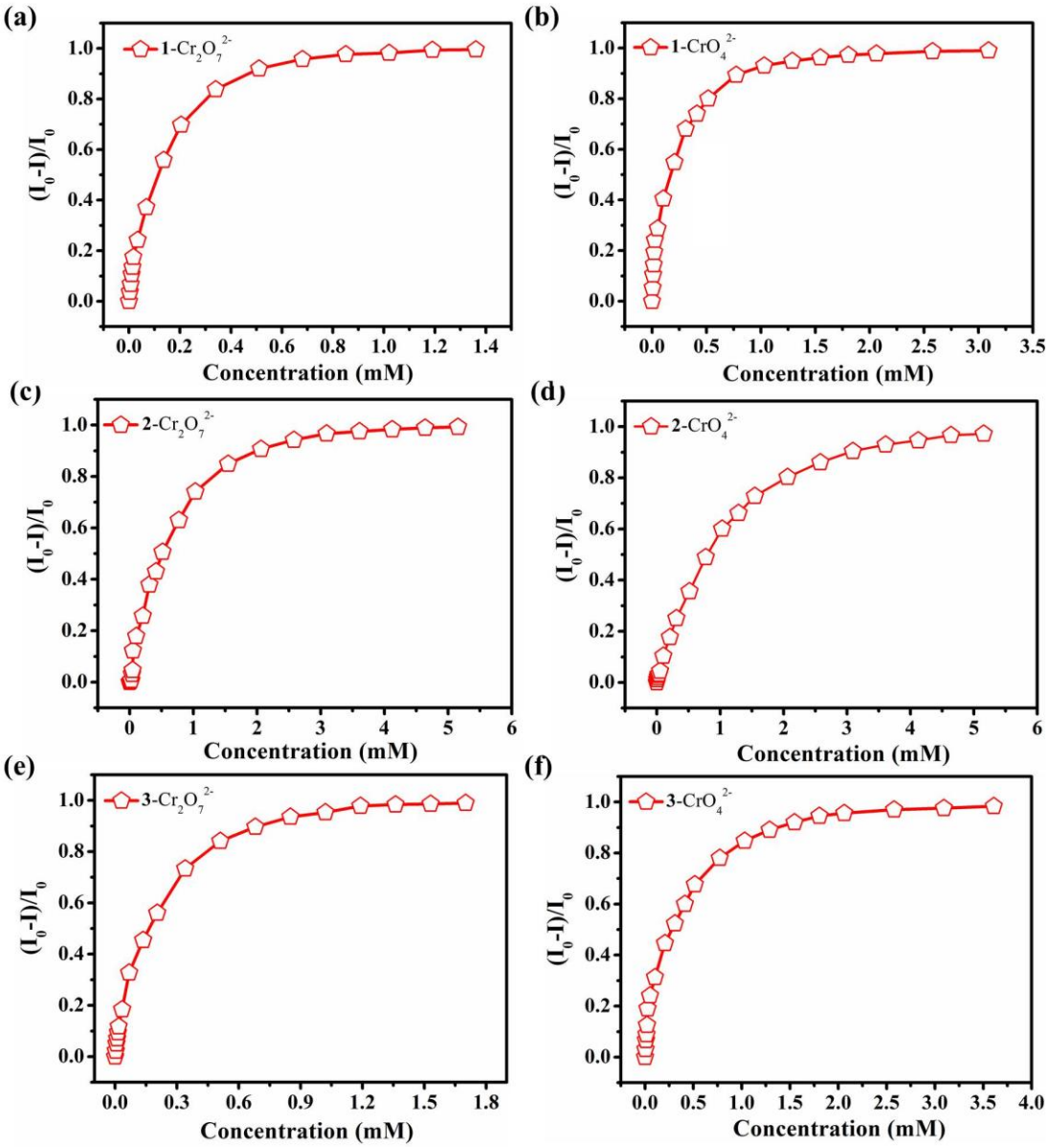

Figure S20. The quenching efficiency of CPs **1** (a) and (b), **2** (c) and (d) and **3** (e) and (f), in aqueous solution with different concentrations of $Cr_2O_7^{2-}$ and CrO_4^{2-} ions.

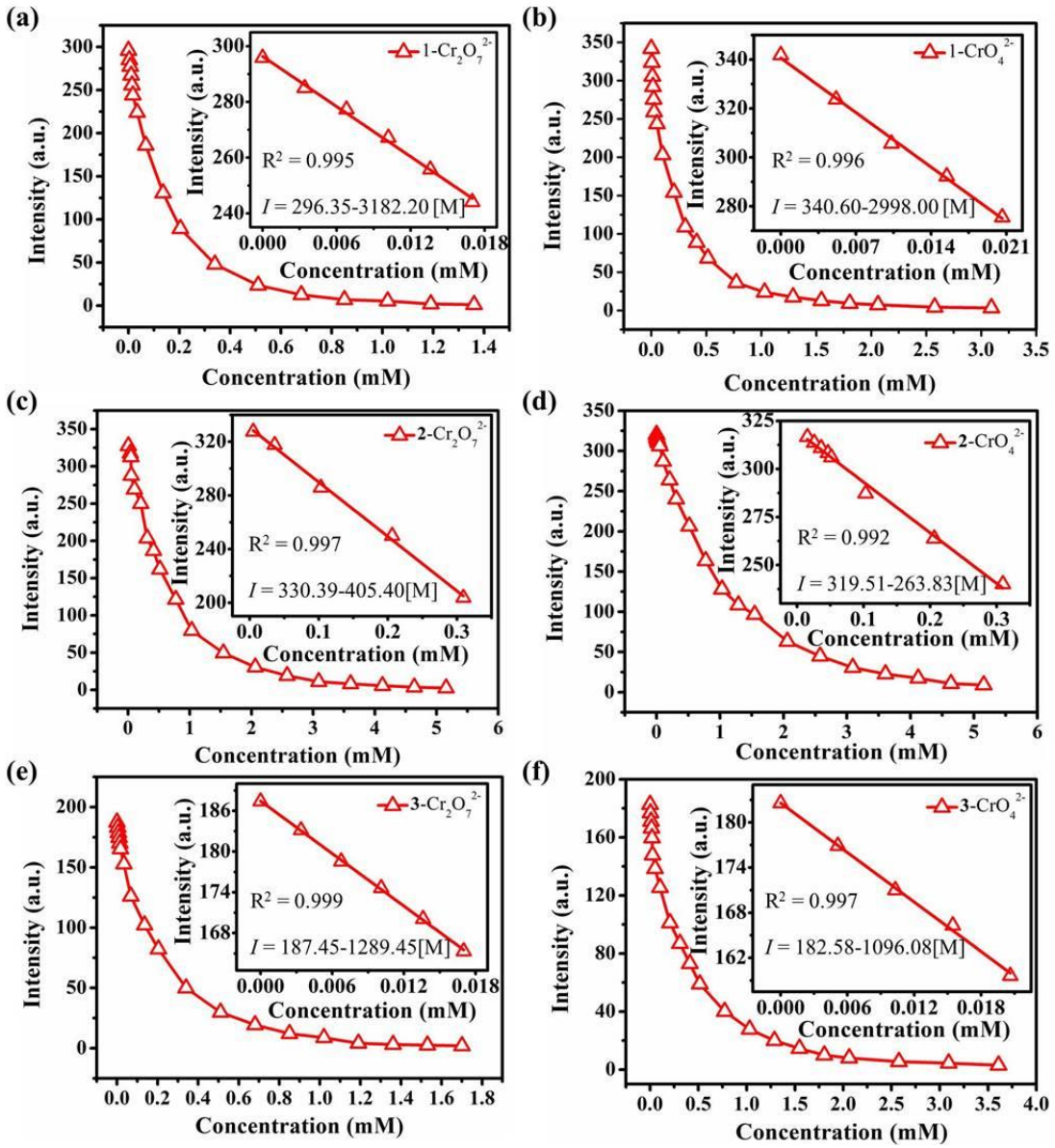

Figure S21. Changes of luminescent intensities with the maximum emission peaks of CPs **1** (a) and (b), **2** (c) and (d) and **3** (e) and (f), in aqueous solution with increasing concentrations of $Cr_2O_7^{2-}$ and CrO_4^{2-} ions, and the linear relationships between intensities and the lower concentrations.

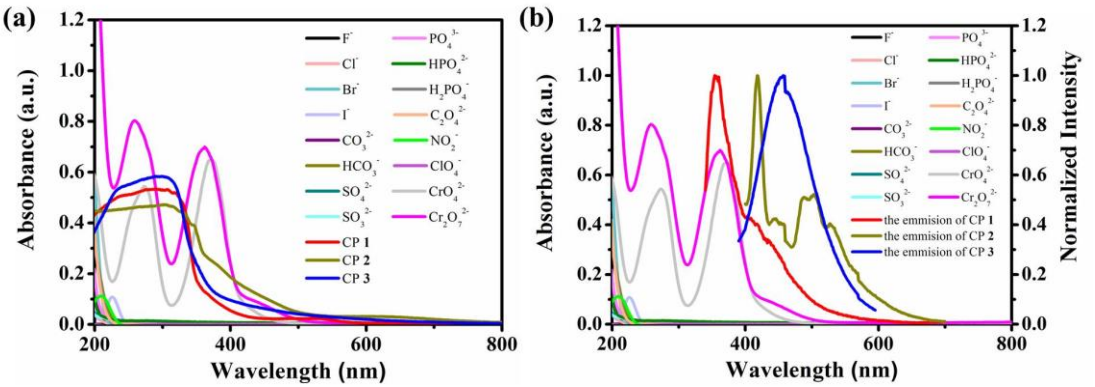

Figure S22. (a) The UV-vis absorption spectra of various anions in their aqueous solutions and the Solid state UV-vis absorption spectra of CPs **1**-**3**; (b) Spectral overlap between the UV-vis absorption spectra of spectra of various anions solutions and emission spectra of CPs **1**-**3** in water.

Table S1. Crystallographic Data and Structure Refinement for **CPs 1-3**.

compound	**1**	**2**	**3**
formula	$C_{18}H_{13}O_5N_2Cd$	$C_{40}H_{22}O_8N_4Cd_2$	$C_{26}H_{26}O_{14}N_2Cd_2$
formula weight	449.70	911.44	815.29
temperature (K)	120(10)	120(10)	120(10)
crystal system	monoclinic	monoclinic	monoclinic
space group	$P2_1/c$	$P2_1/c$	$C2/c$
a (Å)	10.1832(7)	10.2135(4)	7.3297(3)
b (Å)	7.0717(4)	31.3723(11)	18.9428(7)
c (Å)	24.5715(13)	12.9660(7)	20.6050(7)
α (°)	90.00	90.00	90.00
ß (°)	114.484(2)	115.855(3)	89.317(4)
γ (°)	90.00	90.00	90.00
V (Å^3)	1610.34(17)	3738.7(3)	2860.71(19)
Z	4	4	4
D_c, g cm^{-3}	1.855	1.619	1.893
μ, mm^{-1}	1.390	1.195	1.562
F(000)	892.0	1800.0	1616.0
GOF on F^2	1.130	0.989	1.168
R_{int}	0.0382	0.0401	0.0544
R_1, $wR_2[I > 2\ \sigma(I)]$	0.0568, 0.1367	0.0357, 0.0660	0.0612, 0.1454
R_1, wR_2[all data]	0.0650, 0.1417	0.0480, 0.0699	0.0667, 0.1477

Table S2. Selected Bond Lengths (Å) and Angels (deg) of **1**.

Cd(1)-O(1)	2.648(6)	Cd(1)-O(2)	2.285(5)
Cd(1)-O(3)	2.283(5)	Cd(1)-O(4)^{1}	2.325(5)
Cd(1)-O(5)	2.523(5)	Cd(1)-N(1)	2.318(7)
Cd(1)-N(2)	2.354(8)		
O(2)-Cd(1)-O(1)	52.27(18)	O(2)-Cd(1)-O(4)^{1}	82.59(18)
O(2)-Cd(1)-O(5)^{1}	135.06(18)	O(4)^{1}-Cd(1)-O(1)	134.85(18)
O(4)^{1}-Cd(1)-O(5)^{1}	53.75(18)	O(3) -Cd(1)-O(2)	94.67(19)
O(3)-Cd(1)-O(1)	87.1(2)	O(3)-Cd(1)-O(4)^{1}	98.79(19)
O(3)-Cd(1)-O(5)^{1}	83.4(2)	O(5)^{1}-Cd(1)-O(1)	168.37(19)
O(2)-Cd(1)-N(1)	126.6(2)	O(2)-Cd(1)-N(2)	111.2(2)
O(4)^{1}-Cd(1)-N(2)	90.4(2)	O(3)-Cd(1)-N(1)	90.4(2)
O(3)-Cd(1)-N(2)	153.5(2)	N(1) -Cd(1)- O(1)	75.1(2)
N(1) -Cd(1)- O(4)^{1}	148.7(2)	N(1) -Cd(1)- N(2)	70.0(3)
N(1) -Cd(1)- O(5)^{1}	98.3(2)	N(2) -Cd(1)- O(1)	104.0(2)
N(2) -Cd(1)- O(5)^{1}	82.2(2)		

CCDC: 1551327

The asymmetric code: 1: 1+x, +y, +z; 2: -1+x, y, +z; 3: -x, 3-y, -z.

Table S3. Selected Bond Lengths (Å) and Angels (deg) of **2**.

Cd(1)-O(1)	2.303(2)	Cd(1)-O(7)^{1}	2.294(2)
Cd(1)-O(6)^{2}	2.483(2)	Cd(1)-O(5)^{2}	2.315(2)
Cd(1)-N(2)	2.336(3)	Cd(1)-N(1)	2.341(3)
Cd(2)-O(3)^{3}	2.279(3)	Cd(2)-O(2)	2.255(2)
Cd(2)-O(8)^{1}	2.284(2)	Cd(2)-O(4)^{3}	2.420(2)
Cd(2)-N(3)	2.295(3)	Cd(2)-N(4)	2.349(3)
O(1)-Cd(1)-O(6)	90.63(8)	O(1)-Cd(1)-O(5)^{2}	93.36(9)
O(1)-Cd(1)-N(2)	94.01(10)	O(1)-Cd(1)-N(1)	165.60(11)
O(7)^{1}-Cd(1)-O(1)	107.00(9)	O(7)^{1}-Cd(1)-O(6)^{2}	138.13(9)
O(7)^{1}-Cd(1)-O(5)^{2}	86.03(9)	O(7)^{1}-Cd(1)-N(2)	128.65(10)
O(7)^{1}-Cd(1)-N(1)	84.15(11)	O(5)^{2}-Cd(1)-O(6)^{2}	54.61(8)
O(5)^{2}-Cd(1)-N(2)	139.93(9)	O(5)^{2}-Cd(1)-N(1)	96.56(11)
N(2)-Cd(1)-O(6)^{2}	85.97(9)	N(2)-Cd(1)-N(1)	71.70(12)
O(3)-Cd(1)-N(2)	153.5(2)	N(1) -Cd(1)- O(1)	75.1(2)
N(1) -Cd(1)- O(6)^{2}	86.65(9)	O(2)-Cd(2)- O(3)^{3}	89.47(9)
O(2)-Cd(2)-O(4)^{3}	145.42(9)	O(2)-Cd(2)-O(8)^{1}	95.88(9)
O(2)-Cd(2)-N(4)	86.23(10)	O(2)-Cd(2)-N(3)	126.95(9)
O(3)^{3}-Cd(2)-O(4)^{3}	56.00(9)	O(3)^{3}-Cd(2)-O(8)^{1}	108.33(9)
O(3)^{3}-Cd(2)-N(4)	93.04(11)	O(3)^{3}-Cd(2)-N(3)	137.89(10)
O(8)^{1}-Cd(2)-O(4)^{3}	96.97(9)	O(8)^{1}-Cd(2)-N(4)	158.52(10)
O(8)^{1}-Cd(2)-N(3)	90.04(10)	N(4)-Cd(2)-O(4)^{2}	93.14(10)
N(3)-Cd(2)-O(4)^{3}	85.02(9)	N(3)-Cd(2)-N(4)	71.98(11)
CCDC: 1551328			

The asymmetric code: 1: -1+x, -1/2-y, -1/2+z; 2: +x, -1/2-y, -1/2+z; 3: -1+x, +y, +z.

Table S4. Selected Bond Lengths (Å) and Angels (deg) of **3**.

Cd(1)-O(2)^1	2.232(6)	Cd(1)-O(4)^2	2.334(6)
Cd(1)-O(3)^2	2.472(6)	Cd(1)-O(1)	2.409(7)
Cd(1)-O(5)	2.324(7)	Cd(1)-N(1)	2.264(7)
O(2)^1-Cd(1)-O(4)^2	85.6(2)	O(2)^1-Cd(1)-O(3)^2	136.5(2)
O(2)^1-Cd(1)-N(1)	131.1(2)	O(2)^1-Cd(1)-O(1)	95.7(2)
O(2)^1-Cd(1)-O(5)	83.7(2)	O(4)^2-Cd(1)-O(3)^2	54.5(2)
O(4)^2-Cd(1)-O(1)	95.4(2)	N(1)-Cd(1)-O(4)^2	27.3(2)
N(1)-Cd(1)-O(3)^2	89.1(2)	N(1)-Cd(1)-O(1)	86.5(3)
N(1)-Cd(1)-O(5)	88.0(3)	O(1)-Cd(1)-O(3)^2	103.7(2)
O(5)-Cd(1)-O(4)^2	92.4(2)	O(5)-Cd(1)-O(3)^2	81.8(2)
O(5)-Cd(1)-O(1)	172.1(2)		
CCDC: 1551329			

The asymmetric code: 1: -1/2-x, 1/2-y, 1-z; 2: -x, 1-y, 1-z.

Table S5. Hydrogen Bonds (Å) and Angles (°) of Hydrogen Bonds in CP **1.**

D-H···A	d(H···A) (Å)	d(D···A) (Å)	∠D-H···A (°)
O(3)-H(3A)···O(2)	1.93	2.744	157
O(3)-H(3B)···O(4)	1.94	2.728	157
C(11)-H(11)···O(5)	2.39	3.087	130

Table S6. Comparison of Various CPs Sensor for Fe^{3+} ions.

Entry	Material	Analyte	Solution	Ksv (M^{-1})	Detection Limit (M)	Reference
1	$[Eu(L_1)_2(NO_3)]\cdot H_2O$	Fe^{3+}	ethanol		2.6×10^{-5}	S1(d)
2	$\{Eu_2(L_2)_2(HCOO)_2(H_2O)_6\}_n$	Fe^{3+}	DMF	1.58×10^{3}	3.3×10^{-7}	S1(e)
3	$\{[Cd(L_3)(L_4)]\cdot 2H_2O\}_n$	Fe^{3+}	H_2O	3.63×10^{4}	2.21×10^{-6}	S2(b)
	$\{[Cd(L_3)(L_5)(H_2O)]\cdot 0.5H_2O\}_n$	Fe^{3+}	H_2O	3.59×10^{4}	7.14×10^{-6}	
4	$\{[Cd(L_6)(L_7)]\cdot 2H_2O\}_n$	Fe^{3+}	DMF	5.57×10^{4}	2.5×10^{-6}	S3
	$[Zn_2(L_8)_2(L_9)]$	Fe^{3+}	DMF		5.0×10^{-5}	
5	$[Ni(L_8)_2(L_9)_2(H_2O)_2]$	Fe^{3+}	DMF		4.8×10^{-5}	S4
	$[Cd_2(L_8)_2(L_9)(H_2O)]$	Fe^{3+}	DMF		3.6×10^{-5}	
6	$\{[Eu(L_{10})(H_2O)_2]\cdot NMP\cdot H_2O\}_n$	Fe^{3+}	DMF			S5
7	534-MOF-Tb(L_{11})	Fe^{3+}	H_2O	5.51×10^{3}	1.3×10^{-4}	S6
8	$[Eu(HL_{12})(DMF)(H_2O)_2]\cdot 3H_2O$	Fe^{3+}	H_2O	1519		S7
	$[Tb(HL_{12})(DMF)(H_2O)_2]\cdot 3H_2O$	Fe^{3+}	H_2O	4749	5×10^{-5}	
	$[Zn_3(HL_{12})_2(H_2O)_2]\cdot 2DMF\cdot 7H_2O$	Fe^{3+}	H_2O	381.85		
9	CP **1**	Fe^{3+}	H_2O	8.61×10^{3}	1.02×10^{-5}	this work
	CP **2**	Fe^{3+}	H_2O	3.07×10^{3}	2.17×10^{-5}	
	CP **3**	Fe^{3+}	H_2O	6.21×10^{3}	2.03×10^{-5}	

L_1 = 3-(1*H*-pyrazol-3-yl) benzoic acid, L_2 = 9,9-dimethylfluorene-2,7-dicarboxylic acid, L_3 = 4,4'-(2,5-bis (methylthio)-1,4-phenylene) dipyridine, L_4 = 4,4'-biphenyldicarboxylic acid, L_5 = 4,4'-sulfonyldibenzoic acid, L_6 = 5,8-di(1*H*-imidazol-1-yl)quinoxaline, L_7 = 5-hydroxyisophthalic acid, L_8 = 4,4'-oxidibenzoic acid, L_9 = 3,5-bis(5-(pyridin-4-yl)thiophen-2-yl)pyridine, L_{10} = 4,4',4''-striazine-1,3,5-triyltri-m-aminobenzoate, L_{11} = 2,4,6-tris[1-(3-carboxylphenoxy) ylmethyl]mesitylene, L_{12} = 2,8,14,20-tetra-ethyl-6,12,18,24-tetra-methoxy-4,10,16,22-tetra-carboxy-methoxy-calix[4]arene.

Table S7. Comparison of Various CPs Sensor for $Cr_2O_7^{2-}/CrO_4^{2-}$ ions

Entry	Material	Analyte	Solution	Ksv (M^{-1})	Detection Limit (M)	Reference
1	$[Zn_2(L_{13})(L_{14})_2]\cdot 4H_2O$	$Cr_2O_7^{2-}/CrO_4^{2-}$	DMF	$7.59\times10^3/4.45\times10^3$	$3.9\times10^{-6}/4.8\times10^{-6}$	S1(a)
2	$\{[Zn_{2.5}(L_{15})(OH)_2]\cdot solvent_2\}_n$	$Cr_2O_7^{2-}/CrO_4^{2-}$	DMF			S1(b)
3	$\{[Tb(L_{16})]\cdot H_2O\}_n$	CrO_4^{2-}	DMF			S1(c)
4	$[Eu(L_{17})_2(NO_3)]\cdot H_2O$	$Cr_2O_7^{2-}$	ethanol		2.2×10^{-5}	S1(d)
5	$[Zn(L_{18})(L_{19})]_n$	$Cr_2O_7^{2-}/CrO_4^{2-}$	H_2O	$1.37\times10^3/1.00\times10^3$	$1.202\times10^{-5}/1.833\times10^{-5}$	S2(a)
	$[Cd(L_{18})(L_{19})]_n$	$Cr_2O_7^{2-}/CrO_4^{2-}$	H_2O	$2.91\times10^3/1.30\times10^3$	$2.26\times10^{-6}/2.52\times10^{-6}$	
6	$\{[Cd(L_{20})(L_{21})]\cdot 2H_2O\}_n$	$Cr_2O_7^{2-}$	H_2O	6.4×10^3	3.76×10^{-5}	S2(b)
	$\{[Cd(L_{20})(L_{22})(H_2O)]\cdot 0.5H_2O\}_n$	$Cr_2O_7^{2-}$	H_2O	4.97×10^3	4.86×10^{-5}	
7	$[Eu_2(L_{23})_4\cdot CO_3\cdot 4H_2O]\cdot DMF\cdot$ solvent	$Cr_2O_7^{2-}/CrO_4^{2-}$	H_2O	$1.04\times10^4/4.85\times10^3$	$3.64\times10^{-6}/1.70\times10^{-6}$	S8
8	$[Zn(L_{24})]_n$	$Cr_2O_7^{2-}$	DMF			S9
	$[Cd(L_{24})(H_2O)\cdot 2H_2O\cdot CH_3CN]_n$	$Cr_2O_7^{2-}$	DMF			
9	$[Zn(L_{14})(L_{25})]_n$	$Cr_2O_7^{2-}$	H_2O	6555070		S10
10	CP **1**	$Cr_2O_7^{2-}/CrO_4^{2-}$	H_2O	$1.17\times10^4/7.95\times10^3$	$7.38\times10^{-6}/7.79\times10^{-6}$	this work
	CP **2**	$Cr_2O_7^{2-}/CrO_4^{2-}$	H_2O	$2.09\times10^3/1.09\times10^3$	$5.89\times10^{-5}/1.06\times10^{-4}$	
	CP **3**	$Cr_2O_7^{2-}/CrO_4^{2-}$	H_2O	$9.34\times10^3/5.38\times10^3$	$1.36\times10^{-5}/1.60\times10^{-5}$	

L_{13} = tetrakis(4-pyridyloxymethylene)methane, L_{14} = 2-aminoterephthalic acid, L_{15} = 4, 4'-(5-carboxy-1,3-phenylene)bis(oxy)dibenzoic acid, L_{16} = 2,5-di (2',4'-dicarboxylpheny)pyridine acid, L_{17} = 3-(1*H*-pyrazol-3-yl) benzoic acid), L_{18} = isophthalic acid, L_{19} = 3-pyridylcarboxaldehyde nicotinoylhydrazone, L_{20} = 4, 4'-(2,5-bis(methylthio)-1,4-phenylene)dipyridine, L_{21} = 4,4'-biphenyldicarboxylic acid, L_{22} = 4,4'-sulfonyldibenzoic acid, L_{23} = Htpbpc =4'-[4,2';6',4'']-terpyridin-4'-yl-biphenyl-4-carboxylic acid, L_{24} = 4'-(4-(3,5-dicarboxylphenoxy)phenyl)-4,2':6',4"-terpyridine, L_{25} = 4,4'-bis(imidazol-1-ylmethyl)biphenyl.

REFERENCES

S1 (a) Lv, R.; Wang, J.; Zhang, Y.; Li, H.; Yang, L.; Liao, S.; Gu, W.; Liu, X. An amino-decorated dual-functional metal-organic framework for highly selective sensing of Cr(III) and Cr(VI) ions and detection of nitroaromatic explosives. *J. Mater. Chem. A.* **2016**, *4*, 15494-15500. (b) Huang, W. H.; Li, J. Z.; Liu, T.; Gao, L. S.; Jiang, M.; Zhang, Y. N.; Wang, Y. Y. A stable 3D porous coordination polymer as multi-chemosensor to Cr(IV) anion and Fe(III) cation and its selective adsorption of malachite green oxalate dye. *RSC Adv.* **2015**, *5*, 97127-97132. (c) Feng, X.; Li, R.; Wang, L.; Ng, S. W.; Qin, G.; Ma, L. A series of homonuclear lanthanide coordination polymers based on a fluorescent conjugated ligand: syntheses, luminescence and sensor for pollutant chromate anion. *CrystEngComm* **2015**, *17*, 7878-7887. (d) Li, G. P.; Liu, G.; Li, Y. Z.; Hou, L.; Wang, Y. Y.; Zhu, Z. Uncommon Pyrazoyl-Carboxyl Bifunctional Ligand-Based Microporous Lanthanide Systems: Sorption and Luminescent Sensing Properties. *Inorg. Chem.* **2016**, *55*, 3952-3959. (e) Zhou, X. H.; Li, L.; Li, H. H.; Li, A.; Yang, T.; Huang, W. A flexible Eu(III)-based metal-organic framework: turn-off luminescent sensor for the detection of Fe(III) and picric acid. *Dalton Trans.* **2013**, *42*, 12403-12409.

S2 (a) Parmar, B.; Rachuri, Y.; Bisht, K. K.; Laiya, R.; Suresh, E. Mechanochemical and Conventional Synthesis of Zn(II)/Cd(II) Luminescent Polymers Coordination: Dual Sensing Probe for Selective Detection of Chromate Anions and TNP in Aqueous Phase. *Inorg. Chem.* **2017**, *56*, 2627-2638. (b) Chen, S. G.; Shi, Z. Z.; Qin, L.; Jia, H. L.; Zheng, H. G. Two New Luminescent Cd(II)-Metal-Organic Frameworks as Bifunctional Chemosensors for Detection of Cations Fe^{3+}, Anions CrO_4^{2-}, and $Cr_2O_7^{2-}$ in Aqueous Solution. *Cryst. Growth Des.* **2017**, *17*, 67-72.

S3 Zhang, X.; Wang, Z. J.; Chen, S. G.; Shi, Z. Z.; Chen, J. X.; Zheng, H. G. Cd-Based Metal-Organic Frameworks from Solvothermal Reactions Involving in Situ Aldimine Condensation and Highly Sensitive Detection of Fe^{3+} Ions. *Dalton Trans.* **2017**, *46*, 2332-2338.

S4 Han, L. J.; Yan, W.; Chen, S. G.; Shi, Z. Z.; Zheng, H. G. Exploring the Detection of Metal Ions by Tailoring the Coordination Mode of V‑Shaped Thienylpyridyl Ligand in Three MOFs. *Inorg. Chem.* **2017**, *56*, 2936-2940.

S5 Wen, G. X.; Wu, Y. P.; Dong, W. W.; Zhao, J; Li, D. S.; Zhang, J. An Ultrastable Europium(III)-Organic Framework with the Capacity of Discriminating Fe^{2+}/Fe^{3+} Ions in Various Solutions. *Inorg. Chem.* **2016**, *55*, 10114-10117.

S6 Chen, M.; Xu, W. M.; Tian, J. Y.; Cui, H.; Zhang, J. X.; Liu, C. S.; Du, M. A terbium (iii) lanthanide-organic framework as a platform for a recyclable multi-responsive luminescent sensor. *J. Mater. Chem. C.* **2017**, *5*, 2015-2021.

S7 Zhang, S. T.; Yang, J.; Wu, H.; Liu, Y. Y.; Ma, J. F. Systematic Investigation of High-Sensitivity Luminescent Sensing for Polyoxometalates and Iron(III) by MOFs Assembled with a New Resorcin[4]arene-Functionalized Tetracarboxylate. *Chem. Eur. J.* **2015**, *21*, 15806-15819.

S8 Liu, J. J.; Ji, G. F.; Xiao, J. N.; Liu, Z. L. Ultrastable 1D Europium Complex for Simultaneous and Quantitative Sensing of Cr(III) and Cr(VI) Ions in Aqueous

Solution with High Selectivity and Sensitivity. *Inorg. Chem.* **2017**, *56*, 4197-4205.
S9 Wu, Y.; Wu, J.; Luo, Z. D.; Wang, J.; Li, Y. L.; Han, Y. Y.; Liu, J. Q. Fluorescence detection of Mn^{2+}, $Cr_2O_7^{2-}$ and nitroexplosives and photocatalytic degradation of methyl violet and rhodamine B based on two stable metal-organic frameworks. *RSC Adv.* **2017**, *7*, 10415-10423.
S10 Wen, L. L.; Zheng, X. F.; Lv, K. L.; Wang, C. G.; Xu, X. Y. Two Amino-Decorated Metal-Organic Frameworks for Highly Selective and Quantitatively Sensing of Hg^{II} and Cr^{VI} in Aqueous Solution. *Inorg. Chem.* **2015**, *54*, 7133-7135.